Shear behavior of stainless steel girders with corrugated webs

Journal of Constructional Steel Research 210 (2023) 108086

Contents lists available at ScienceDirect

Journal of Constructional Steel Research

journal homepage: www.elsevier.com/locate/jcsr

Shear behavior of stainless steel girders with corrugated webs

Mozhdeh Amani [a,*], Mohammad Al-Emrani [a], Mathias Flansbjer [b]

[a] Department of Architecture and Civil Engineering, Chalmers University of Technology, SE-412 96 Gothenburg, Sweden
[b] Chemistry and Applied Mechanics, RISE Research Institutes of Sweden, SE-501 15 Borås, Sweden

ARTICLE INFO

Keywords:
Corrugated web girders
Stainless steel
Shear strength
Imperfection sensitivity

ABSTRACT

In this paper, the shear strength of corrugated web girders made of EN 1.4162/LDX 2101 stainless steel is investigated. Four full-scale trapezoidal corrugated web girders were tested under shear. Before conducting the tests, DIC was used to measure the real geometric imperfections in the web panels. Complementary finite element analysis studies were conducted to assess the sensitivity of the shear strength to initial imperfections. The experimental results indicated that all the tested girders with a local slenderness ratio of $\lambda = 0.7$ attained the shear yield strength, which was then followed by strain hardening in the material at a level that was 8–18% higher than the yield strength. This implies that the Eurocode's limit of $\lambda = 0.25$ to attain the plastic shear strength in corrugated webs can be quite conservative for stainless steel. According to the findings of the imperfection sensitivity studies, an initial geometric imperfection based on the first eigen buckling mode and with a maximum amplitude of $a_{max}/200$, where a_{max} is the maximum corrugation fold length, yielded ultimate strength within 3% of the test results. When the amplitude was increased to $h_w/200$, where h_w is the web height, the ultimate strength was estimated to be 25% lower on average than in the experiments. In three of the studied girders, initial imperfections with other forms than the first buckling mode were found to be more critical. Further, it was found that regardless of mode number, mode shapes that are more extended over the web panel result in a higher degradation of the ultimate shear strength.

1. Introduction

Modern steels with enhanced performance have been available for decades, with the potential to address the issue of sustainability better than conventional steels. In this sense, stainless steel is one of the most interesting materials. The superior corrosion resistance of stainless steel offers enhanced durability and low maintenance costs during the service life of bridges. The findings of rigorous life-cycle cost (LCC) and life-cycle assessment (LCA) analyses show that stainless steel bridges can save 30–40% in life-cycle costs compared to conventional carbon steel over a 60-year service life [17]. Savings of up to 50% can be realized after 100–120 years of service ([18,19].

Stainless steel comes in four types: martensitic, ferritic, austenitic, and austenitic-ferritic. Austenitic-ferritic grades, which are known as duplex stainless steels, have been used in bridges since they are mechanically stronger than either ferritic or austenitic types. The new lean duplex steels stand out within the duplex family for their comparable strength to duplex grades and high corrosion resistance at a lower cost. Consequently, the use of lean duplex steel in bridge construction is becoming more common [14].

In addition to its superior corrosion resistance, stainless steel has a high strength-to-weight ratio, which allows for material savings with the potential to create architecturally and aesthetically more desirable design solutions. Despite these benefits, the potential of employing stainless steel in bridge construction is yet underutilized. One reason might be a lack of knowledge and understanding of stainless steel and its structural behavior [14]. The high cost of stainless steel, on the other hand, seems to be a major hindrance to its extensive application in bridges, which consume massive quantities of materials ([13,17].

This paper is the outcome of research conducted as part of the "*SunLight*" project (Acknowledgement), which aimed to minimize the initial cost of stainless steel bridges by using the potential of corrugated web girders. The use of corrugated web plates in steel girders allows the increase of the shear capacity without the need to increase the thickness of the web plate or use excessive transverse stiffeners. Consequently, this design solution has the potential to reduce the amount of needed material and welds, which is particularly important for stainless steel because of its higher price than carbon steel. It is worth mentioning that

* Corresponding author.
E-mail address: mozhdeh.amani@chalmers.se (M. Amani).

https://doi.org/10.1016/j.jcsr.2023.108086
Received 13 February 2023; Received in revised form 30 May 2023; Accepted 16 June 2023
Available online 24 June 2023

trapezoidal and sinusoidal corrugations are the most common shapes of corrugation and a trapezoidal corrugation profile in shown in Fig. 1.

The bending moment and shear force in a corrugated web beam are handled separately by the flanges and the web, respectively, due to what is usually referred to as the "accordion effect," which is also recognized by design standards such as Eurocode 1993-1-5. This means that while investigating the shear behavior of a corrugated web, there is no need to investigate the interaction with the bending moment. Meanwhile, the design model for calculating the shear strength of corrugated webs in EN-1993-1-5 was developed based on tests on beams made of carbon steel in the range of the yield strength between 190 and 690 *MPa* [7]. However, stainless steel shows higher levels of ductility and strain hardening than carbon steel, and the stress-strain curve in stainless steel is not the same as that in carbon steel. Stainless steel has a more rounded response with no well-defined yield strength, while carbon steel typically displays linear elastic behavior up to the yield strength and a plateau before strain hardening occurs [1].

To the knowledge of the authors, the shear behavior of corrugated web stainless steel girders is being studied for the first time in the current research, the question arises whether the existing design model in Eurocode is also applicable to girders made of stainless steel or whether there is a need to revise the design model and, perhaps, make better use of stainless steel.

2. Theoretical background and literature review

Shear failure in a corrugated web beam can occur because of either local buckling within the corrugation folds or global buckling of the entire web panel. In beams with stocky webs, the plastic shear strength can be reached due to material yielding without any shear buckling instability. In local buckling, the web acts as a combination of flat and inclined folds that mutually support each other along their vertical edges while being supported by the flanges along their top and bottom edges. In principle, local buckling includes one or more single folds, but the buckling half-waves do not cross the fold intersections. The isotropic plate stability theory may be used to estimate the elastic local shear buckling stress of a single fold according to Eq. (1).

$$\left(\tau_{cr,l}\right)_{el} = k_l \frac{\pi^2 E}{12(1-\upsilon^2)} \left(\frac{t_w}{a_{max}}\right)^2 \tag{1}$$

Where t_w is the web plate thickness and a_{max} is the maximum fold length, see Fig. 1. E and υ are the Young's modulus of elasticity and the Poisson's ratio, respectively. The local buckling coefficient, k_l, depends on the boundary conditions and the fold aspect ratio. Numerous previous investigations have demonstrated that the boundary condition at the web-flange junction is closer to fixed owing to the fairly large difference in thicknesses of the common plates in the web and flanges, e.g., [5]. However, by ignoring the fixity effects and employing the buckling coefficient for simply supported folds acting as long plates, lower bound results are assured ([2,7].

On the other hand, in global buckling, the entire web panel is treated as an orthotropic flat plate with different bending stiffness in different directions. In this mode of failure, the buckling half-waves spread over multiple adjacent folds and extend diagonally over the entire height of the web. The orthotropic plate stability theory may be used to estimate the elastic global shear buckling stress according to Eq. (2).

$$\left(\tau_{cr,g}\right)_{el} = \frac{k_g}{t_w h_w^2} \sqrt[4]{D_x D_z^3} \tag{2}$$

D_x and D_z are the plate bending stiffnesses about the weak and strong axes, respectively, which are calculated per unit length of the web according to Eqs. (3) and (4), respectively. w is the length of one-half wave of the corrugation, and s is the unfolded length of one half-wave, Fig. 1. I_z is the second moment of area of one corrugation of length w, about the corrugation centerline and is given by Eq. (5). h_w is the height of the web plate. For the global buckling coefficient, k_g, with the same reasoning as for local buckling, assuming a simply supported boundary condition and applying the relevant buckling coefficient results in improved safety.

$$D_x = \frac{E t_w^3}{12(1-\nu^2)} \frac{w}{s} \tag{3}$$

$$D_z = \frac{E I_z}{w} \tag{4}$$

$$I_z = \frac{t_w}{12} a_3^2 (a_2 + 3a_1) \tag{5}$$

According to [3], if any of the elastic stresses calculated using the above equations, whether for local buckling or for global buckling, is greater than 80% of the shear yield stress, $0.8\tau_y$, the effect of the material yielding on the shear strength should be considered. In such cases, the inelastic buckling stresses can be calculated using Eq. (6), where the maximum stress is limited to the shear yield stress.

$$\left(\tau_{cr}\right)_{inel} = \sqrt{0.8\tau_y \left(\tau_{cr}\right)_{el}} \le \tau_y \tag{6}$$

The critical shear stress might be obtained as the least value among the stresses calculated from Eqs. (1) and (2), including the effect of material yielding on stresses in the case of inelastic buckling according to Eq. (6). But large discrepancies between the theoretically anticipated stresses, according to what can be calculated based on the above-mentioned equations, and the results of shear tests conducted on corrugated web beams have been reported in several previous research studies. This discrepancy might be caused by neglecting some factors that influence the shear buckling behavior, which could result in a significant loss of safety according to ([2,16].

A study of published works in the field shows that the occurrence of interactive buckling in corrugated web plates has been pointed out as one possible reason for the discrepancy between the theoretically calculated critical buckling stresses and those obtained from testing. In

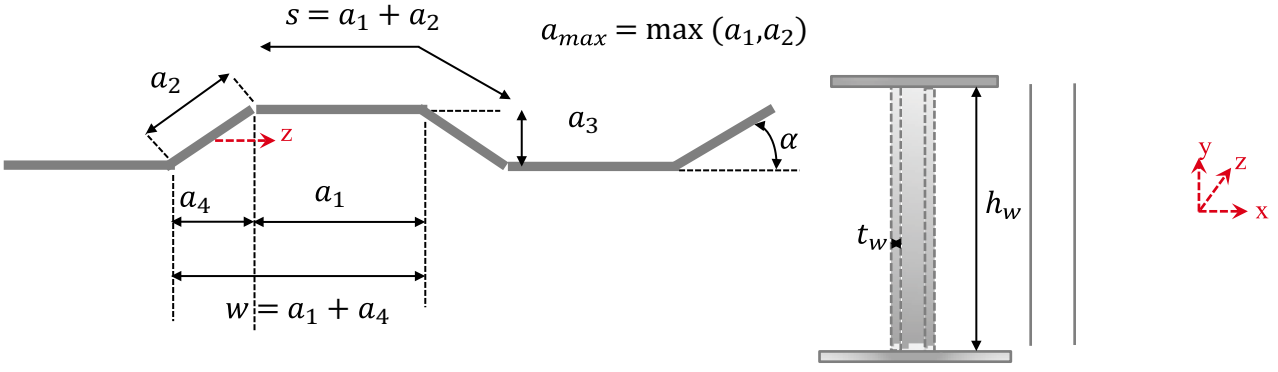

Fig. 1. Geometric parameters of a web with trapezoidal corrugation.

an interactive buckling mode, the local buckling half-waves cross the fold intersections and expand on more than a single fold, and numerous half-waves may form in the web height. Several scholars presented analytical equations for calculating an interactive shear buckling stress, $\tau_{cr,I}$, based on test data and finite element analyses. The following framework may be used to represent most of the suggested models, albeit with distinct values for the two parameters, n and u.

$$\frac{1}{(\tau_{cr,I})^n} = \frac{1}{(\tau_{cr,l})^n} + \frac{1}{(\tau_{cr,g})^n} + \frac{u}{(\tau_y)^n} \tag{7}$$

If the effect of material yielding on the shear buckling strength is considered, then u is other than zero, and depending on the specified upper limit for the stress ($\tau_{cr,I}$), its value may be 1 or greater. [15] have set the upper limit of $\tau_{cr,I} = 0.8\tau_y$ for the stress owing to a lack of test data to validate the potential for achieving the material yield stress as a corrugated web becomes stocky. However, shear yield stress in corrugated web beams with low slenderness ratios has been observed in several shear tests ([9–11]. There should also be a note that different studies have come up with different numbers for n.

In addition, previous research reveals that the shear strength of corrugated webs is highly sensitive to initial imperfections. This can be another key factor for the considerable dispersion of shear strength of corrugated web beams in the conducted tests ([2,12,15]. Initial imperfections refer to residual stresses and geometric shape imperfections that are produced during the manufacturing of welded beams with corrugated webs. Despite their importance, information of residual stresses and exact geometric imperfections, particularly for corrugated web girders, is limited according to [8]. EN 1993-1-5 [20] suggests using *equivalent* local and global geometric imperfections to include the effects of initial imperfections of both types, i.e., residual stresses and geometric imperfections. For a flat web girder, a global imperfection in the form of an initial bow with an equivalent amplitude of $h_w/200$ is recommended. However, geometric imperfections seem to be smaller in a corrugated web plate than in a flat plate due to the stiffening effect of the corrugations in the out-of-plane direction. Moreover, even though there are no test-based equivalent geometric imperfections for corrugated web plates, [8] concluded that the magnitude of equivalent geometric imperfections is often significantly smaller than $h_w/200$. For panels or subpanels, a local imperfection based on the critical plate buckling mode shape and an amplitude equal to the minimum dimension of the critical sub-panel divided by 200, $a_{max}/200$, is recommended by EN 1993-1-5.

[2] investigated the effects of initial imperfections in the form of the lowest 49 eigenmodes found via linear buckling analysis, with an amplitude equal to the plate thickness, $t_w = 6\ mm$. They concluded that the shear strength rises with the mode number, with the first mode providing the most crucial condition. They showed that by considering the initial geometric imperfection based on the first buckling mode and with an amplitude equal to the plate thickness, the shear capacity is lowered by 23% compared to the shear yield strength. Furthermore, they demonstrated that the shear yield strength may be achieved by restricting the amplitude of the geometric imperfections to a maximum of 10% of the plate thickness. It is worth noting that the maximum amplitude of geometric imperfections considered in their studies is based on measurements made by both manual and electronic methods before the experiments. It should also be highlighted that they recommended an upper limit on the ratio of web depth to thickness to avoid global buckling and subsequent substantial shear strength loss in corrugated web plates. Their conducted test findings verified the occurrence of local buckling.

[4] studied the shear behavior of corrugated web beams made of high-strength steel. They found that the interactive equation suggested by [15] can best predict the capacity. In their studies, they assumed initial imperfections based on the first buckling mode and with an amplitude of $h_w/200$.

[12] studied the effects of initial geometric imperfections with a shape based on the first elastic shear buckling mode and with different amplitudes varying in the range of $h_w/1000 - h_w/100$. They showed that the sensitivity of the shear strength of corrugated web beams to initial imperfections is not very high when buckling occurs before yielding in shear, i.e., when buckling is elastic. This is attributed to the membrane effect when shear buckling governs the failure. In other words, when the web deforms in the out-of-plane direction because of shear buckling before the shear yield, the membrane effect's contribution to increasing the web shear strength can make the ultimate load less sensitive to the initial geometric imperfections. On the other hand, when buckling is preceded by web yielding, the sensitivity to initial imperfections is high.

2.1. EN 1993-1-5 shear force design model

In EN 1993-1-5 [20], a simply supported boundary condition is assumed and, by employing the local and global buckling coefficients of 5.34 and 32.4, respectively, the local and global critical stresses are provided by Eqs. (8) and (9).

$$\tau_{cr,l} = 4.83\ E\left(\frac{t_w}{a_{max}}\right)^2 \tag{8}$$

$$\tau_{cr,g} = \frac{32.4}{t_w h_w^{\,2}}\sqrt[4]{D_x D_z^{\,3}} \tag{9}$$

After calculating the critical stresses, the slenderness parameters related to both local and global buckling modes are calculated using Eqs. (10) and (11).

$$\bar{\lambda}_{c,l} = \sqrt{\frac{f_{yw}}{\tau_{cr,l}\sqrt{3}}} \tag{10}$$

$$\bar{\lambda}_{c,g} = \sqrt{\frac{f_{yw}}{\tau_{cr,g}\sqrt{3}}} \tag{11}$$

f_{yw} is the yield strength of the web plate. The interactive buckling mode is not considered in EN 1993-1-5. The reasoning is that the likely interaction is so *weak* that checking the local and global buckling modes separately would be acceptable. This idea was originally proposed by [6] and later backed by [7]. Based on this, upon having the separate slenderness parameters, the reduction factors for local and global buckling, respectively, should be calculated by Eqs. (12) and (13), and the minimum of them, denoted by χ_c should be applied in Eq. (14) to calculate the characteristic shear resistance.

$$\chi_{c,l} = \frac{1.15}{0.9 + \bar{\lambda}_{c,l}} \le 1 \tag{12}$$

$$\chi_{c,g} = \frac{1.5}{0.5 + \bar{\lambda}_{c,g}^{\,2}} \le 1 \tag{13}$$

$$V_R = \chi_c \frac{f_{yw}}{\sqrt{3}} h_w t_w \tag{14}$$

The local and global buckling factors in Eqs. (12) and (13) are graphically depicted in Fig. 2 as a function of the slenderness.

According to Fig. 2, the shear yield strength should be reached for slenderness values less than $\lambda = 0.25$. However, in comparison to other buckling problems, this limit for corrugated webs is seen to be quite conservative, although further experimentation is required to verify this statement [7]. On the other hand, when the material yields before buckling, the shear resistance is very sensitive to initial imperfections, as stated by, e.g., [12]. Consequently, it is seen that the buckling strength is reduced relative to the yield strength in the medium range of slenderness.

It is worth mentioning that there is no update for stainless steel in the Eurocodes' shear strength design model for corrugated web beams. The

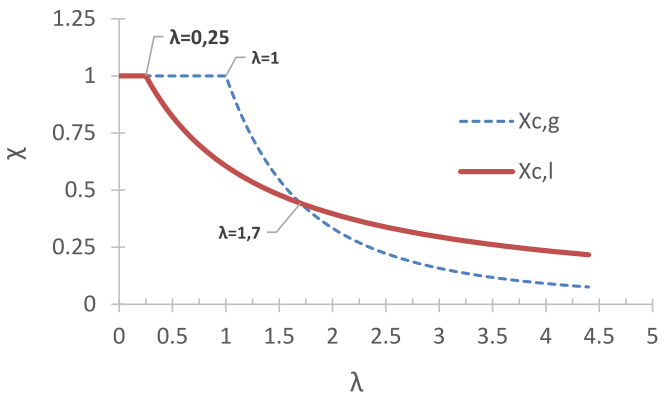

Fig. 2. EN 1993-1-5 local and global buckling factors for a corrugated plate as a function of the web slenderness.

modulus of elasticity, E, the Poisson's ratio, υ, and the yield strength, f_{yw}, are the material-dependent parameters in Eqs. (8) to (11), which can be determined according to EN 1993-1-4 [21]. EN 1993-1-4 recommends a value of 200 × 10^3 N/mm^2 for the modulus of elasticity for different standard grades of duplex stainless steel commonly used in structural applications [1]. Moreover, the reduction factors in Eqs. (12)–(14) are determined based on the tests conducted on carbon steel with no consideration of strain hardening in the material. Therefore, these reduction factors, which are functions of the slenderness ratios, would be different for stainless steel.

3. Method of study

As stated earlier in the introduction, the aim of the current research study is to evaluate the shear behavior of stainless steel corrugated web girders in comparison to the Eurocode's shear strength design model, which, as mentioned in the introduction, is developed based on carbon steel. The research is implemented in two phases of experimental and finite element studies. In the first phase, four corrugated web girders (Labeled 1001–1004) with dimensions close to those common in composite road bridges are produced and tested in three-point bending to investigate their shear capacity. The girders are made of EN 1.4162/LDX 2101 stainless steel and have different sets of geometric corrugation parameters as introduced in Table 1 (Fig. 1).

The length of the flat and inclined panels of the corrugation, a_1 and a_2, the length of one-half wave (w), and the unfolded length of one half-wave (s) for each girder are given in Table 1. The angle of the corrugation in degrees is denoted by α. The ratio (s/w) indicates the length of the plate used to produce the corrugated web per unit length along the girder. Therefore, higher values of s/w indicate more material consumption in the girder's web for a given web thickness and depth.

The girders are tested in three-point bending with a simply supported boundary condition at the ends and a load applied in the middle of the span. They have a span length between 3.8 and 4.0 m and a height between 1.35 and 1.45 m. The top and bottom flange dimensions (250 × 25 mm^2) eliminated the risk of flange buckling and early yielding in bending. The lateral-torsional buckling mode of failure is prevented by applying lateral restraints at both supports and at the point of load application. In addition, 10 mm and 20 mm thick stiffeners are attached at the supports and under the point load, respectively, to avoid the risk of local failure under concentrated forces.

Due to the placement of measuring equipment during the testing on one side of the girders, the thickness of the web is different on both sides of the load, 4 mm and 6 mm, to limit the location of the shear failure to one panel (the thinner web plate). An overview of the test setup is shown in Fig. 3.

Table 1
Corrugation parameters of the tested girders.

Girder's label	a_1-a_3-α:	a_2 (mm)	a_{max} (mm)	s (mm)	w (mm)	s/w
1001	170-60-35	104.61	170	274.6	255.7	1.074
1002	170-60-45	84.85	170	254.8	230	1.11
1003	170-100-35	174.34	174.34	344.3	312.8	1.1
1004	170-100-45	141.42	170	311.4	270	1.15

3.1. Details of boundary conditions and loading in the conducted tests

The girder is placed on two rollers with a center distance of 3.6 m. A steel plate (250 × 250 × 20 mm) is placed between the roller and the bottom flange at both supports. One of the supports can tilt to compensate for possible small non-straightness of the bottom flange. The supports are also provided with end stops to prevent the girder from rolling of the support at failure. Fork supports are used to avoid the upper flange from moving laterally at the ends. The roller and lateral fork supports are shown in Fig. 4a-c. The longitudinal movement is allowed using Teflon sheets between the flange and the fork support (Fig. 4b). The load is applied through a spherical bearing that is placed on top of a steel plate (250 × 250 × 40 mm) to distribute the load to the upper flange and the vertical stiffeners (Fig. 4d). The upper flange is laterally supported by a fixture connected to the loading cylinder. In addition, the bottom flange is also laterally supported, as shown in Fig. 4e.

The tests are performed in a servo-hydraulic testing machine with a maximum capacity of 20 MN. The load is applied quasi-statically in displacement control with a 1.2 mm/min rate. The tests are conducted in the following loading sequence: 1) Initial preload of 10 kN, 2) loading to 500 kN, 3) unloading to 10 kN, and 4) loading to failure. During testing, the mid-span deflection of the girder is measured using linear variable displacement transducers (LVDT), shown in Fig. 4e, with a measuring range of 100 mm, while transducers with a 50 mm measuring range, shown in Fig. 4f, are used to measure the support setting displacements. The displacements are measured relative to the supporting steel table of the test machine. The MTS measuring system acquired the load and displacement values with a frequency of 10 Hz.

3.2. Strain measurement

Strains are measured during the tests with general-purpose strain gauges from Kyowa with a gauge length of 5 mm: KFGS 120 Ω Uniaxial strain gauges and KFGS 120 Ω Triaxial, 0°/90°/45° stacked rosette strain gauges. All the four girders are provided with two uniaxial strain gauges placed at the mid-span of the bottom flange (one gauge at each side of the web) and one triaxial strain gauge in each of the two web panels. In addition, girder 1001 is provided with two extra uniaxial strain gauges at the bottom flange (ax-3, ax-4) and top flange (ax-5, ax-6). The axial gauges are placed at the upper surface of the flanges, 10 mm from the longitudinal flange edge. The position of the strain gauges in 1001 is presented in Fig. 5. The strains are acquired with HBM Quantum at a frequency of 10 Hz.

3.3. Optical full field deformation measurement

The thinner web panel's full field geometry and deformations are monitored by 3D-DIC using the optical system ARAMIS 12 M. The DIC system is calibrated for a measurement volume of approximately 1700 × 1370 × 1370 mm^3. The speckle pattern is achieved by first applying white retro-reflective paint as a background on the web panel, then applying black stains using a rough plastic brush. Before testing, the DIC system is used to scan the initial geometry and imperfections of the web

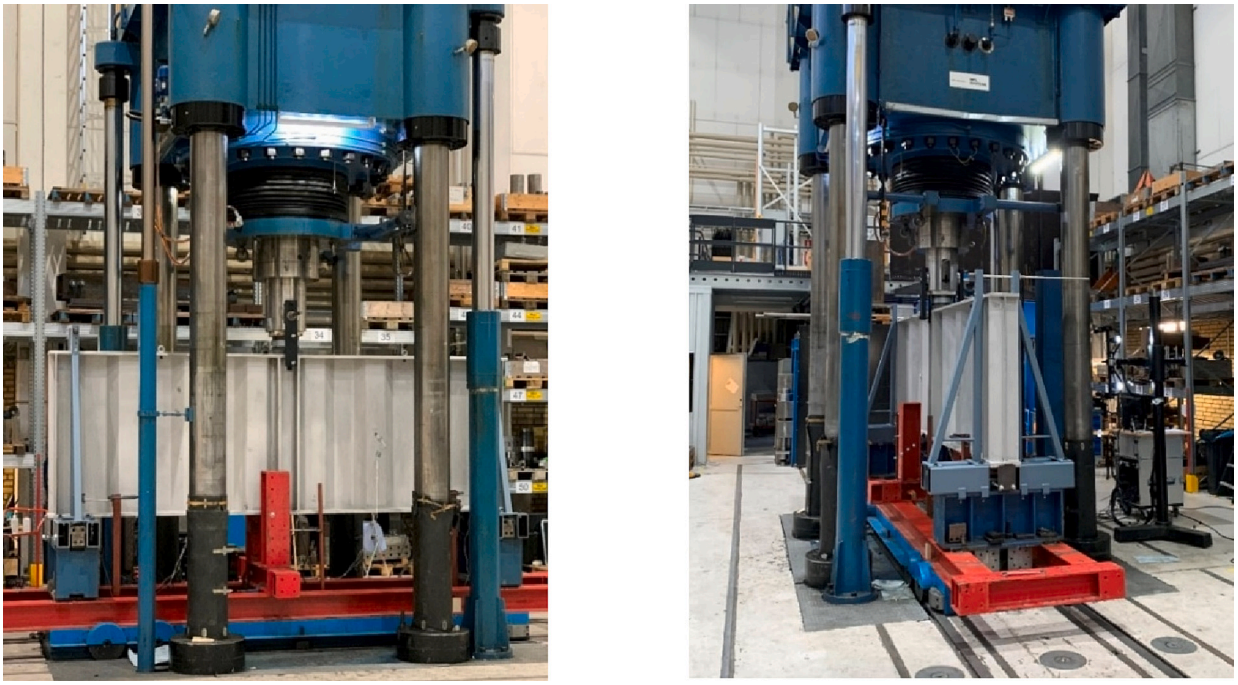

Fig. 3. Overview of three point bending test setup (1004).

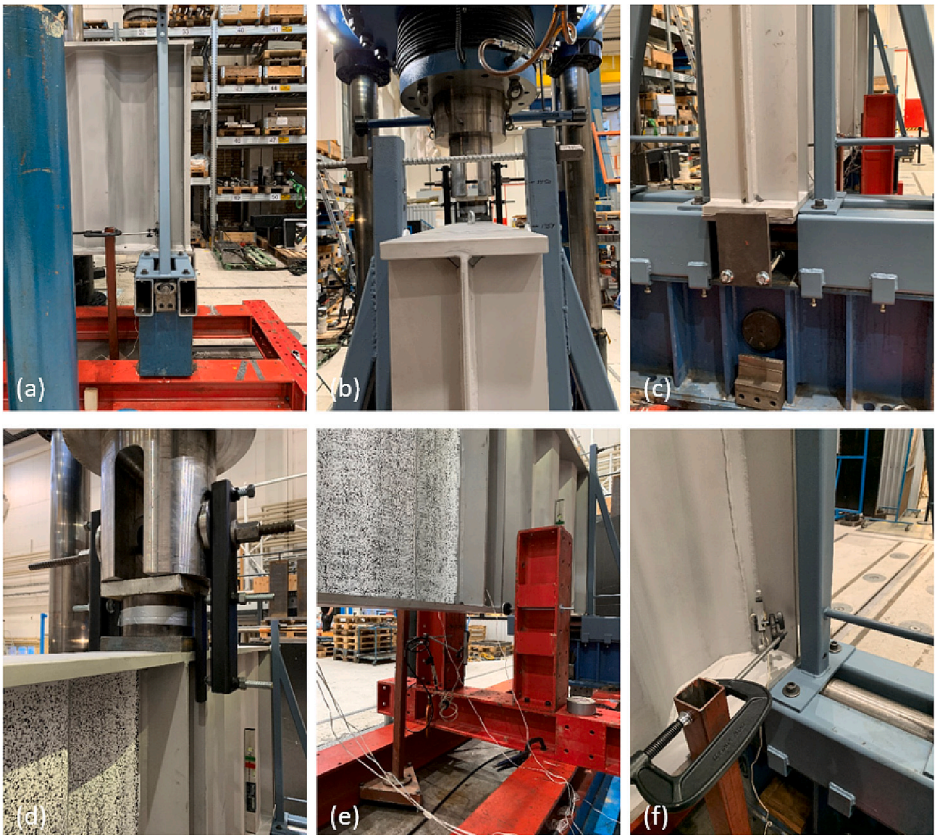

Fig. 4. Details of the three- point bending test setup (1004): (a-c) roller support with lateral fork support, (d) loading point with spherical bearing and lateral support of upper flange, (e) lateral support of lower flange and LVDT measuring the mid-point displacement, and (f) LVDT measuring the support displacement.

panel (Fig. 6a). During testing, the camera sensors are oriented in a vertical direction to maximize the field of view due to the restrictions in space caused by the loading frame of the machine (Fig. 6b). The image frequency is 0.5 Hz during the first load cycle and then increased to 1 Hz during the failure loading sequence up to the initiation of web buckling. A manually triggered image loop recording of 10 Hz is used to capture the web buckling development at failure. The load and displacement from the testing machine are simultaneously recorded in the DIC system.

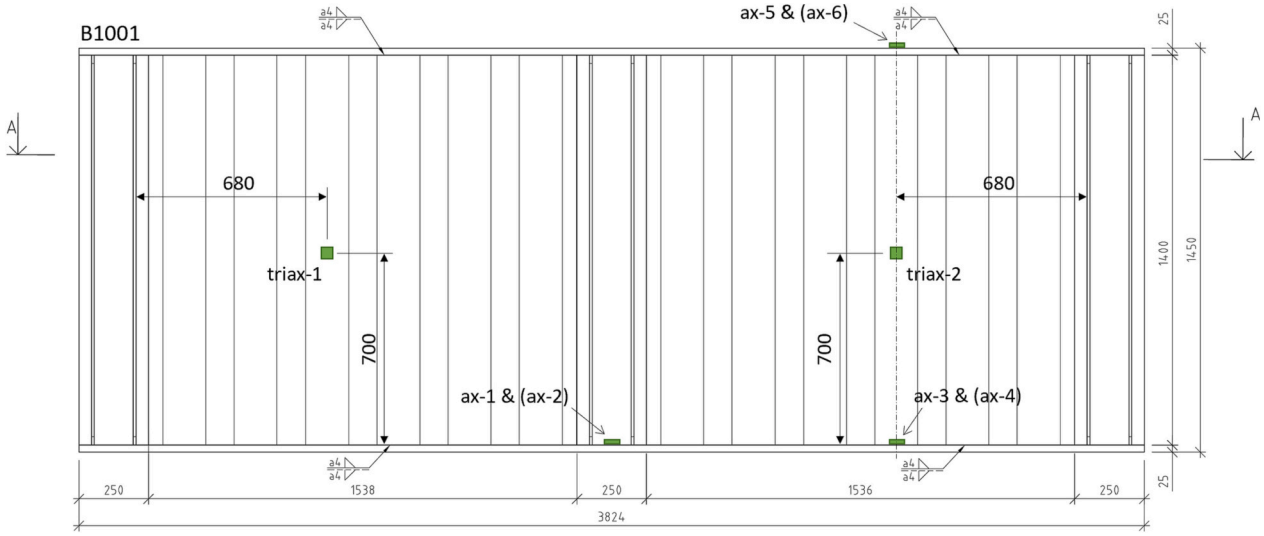

Fig. 5. Positions of strain gauges in girder 1001. The uniaxial gauges given in parentheses are mounted at the opposite side of the girder.

a ***b***

Fig. 6. Setup of optical full field deformation measurement (a) at scanning before test and (b) during three-point loading test.

A sub-set size of 15 × 15 pixels and a sub-set step of 10 pixels are chosen. This corresponds to a grid resolution of approximately 4.3 × 4.3 mm for the system setup employed. The coordinate measurement accuracy is better than 0.01 mm in the plane (x, y) and 0.02 mm out-of-plane (z).

In the second phase of the studies, finite element analyses are conducted with the aim of providing a validated FE tool to analyze the effect of initial geometric imperfections on the shear capacity. Therefore, in the first step of FE studies, having obtained the accurate measured data from the tests, the experiments are simulated using a fully material and geometric nonlinear finite element method. Using the STL Import tool in ABAQUS, the DIC measured real geometry of the thinner web plate was imported first as an *orphan mesh* and then converted into a *part*. However, the coordinates of the edge nodes are modified due to the low accuracy of DIC measurements at the boundaries. Other elements of the girder, such as flanges, stiffeners, and the thicker web plate, are modeled geometrically perfect. The finite element results in this step are compared against the test results to validate the Finite Element Modeling approach. In the next step, the whole girders are modeled with no initial imperfections. Following that, the eigen buckling modes are extracted using a linear buckling analysis. To evaluate the imperfection sensitivity, nonlinear analysis method is employed including the initial geometric imperfections based on the extracted buckling modes with different amplitudes.

S3, a 3-node triangular general-purpose shell element, is used to model the entire girder. Due to the 2.5 mm size of DIC mesh, the same size is used for the FE mesh in the thinner web. The mesh size in the areas with a perfect geometry is 10 mm. It is ensured that the mesh sizes are sufficient to achieve convergence of the results. It is worth noting that the different elements of the girder (i.e., flanges, web, stiffeners) are connected using tie interaction constraint.

3.4. Material properties

As previously stated, EN 1.4162/LDX 2101 lean duplex stainless steel is used in the current study. However, it is known that residual stresses due to cold forming operations in the fabrication of corrugated plates can affect the material properties. Therefore, tensile tests are conducted on specimens taken from the web plate's flat and bent areas according to the EN ISO 6892-1 standard. The results are shown in Fig. 7. It is observed that while the ultimate stress is higher in the bent area, the ultimate tensile strain, which indicates ductility, is lower in the bent area than in the flat part of the web. To investigate the influence of this

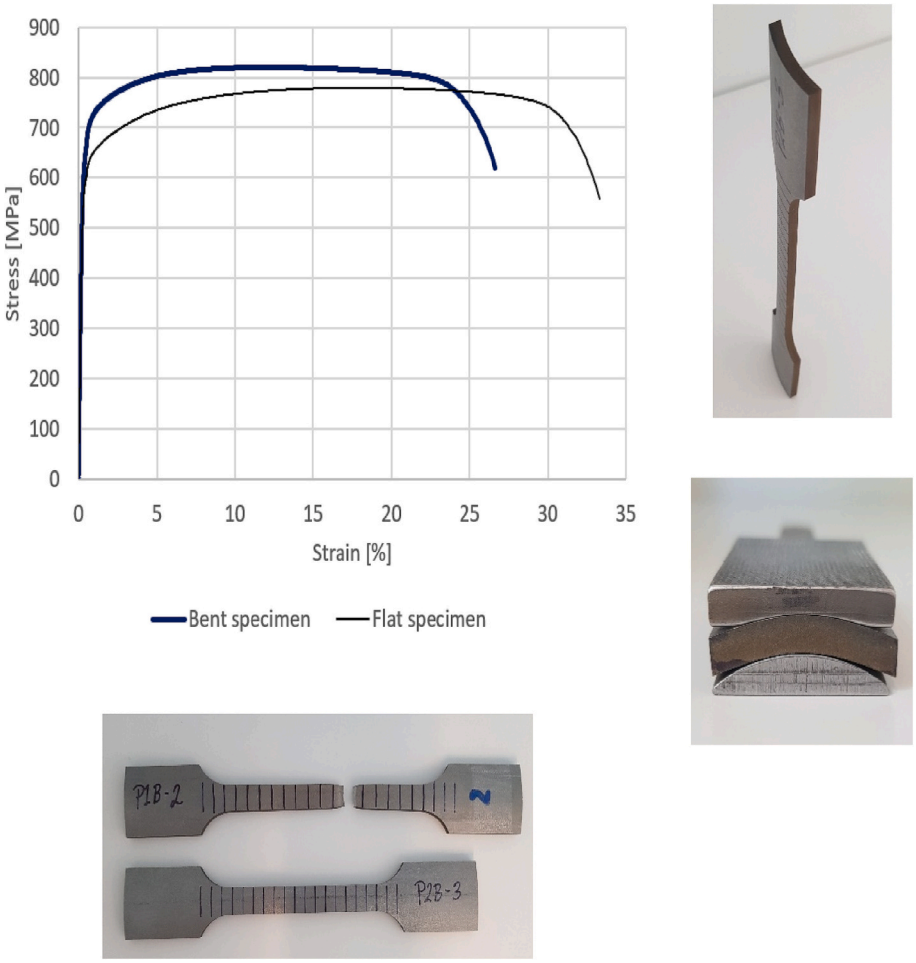

Fig. 7. Material test specimens and the engineering stress-strain curve for EN 1.4162/LDX 2101 stainless steel in the web plate obtained in the current research project.

local change in material properties, the shear behavior of girders, with and without account taken for the change in material characteristics in the bent zone, is compared. Based on the results of this sensitivity analysis, it is concluded that the strain hardening effect in the bent regions does not influence the behavior and strength of the girders and can thus be neglected. It is worth mentioning that the *engineering* stress-strain curve in Fig. 7 are converted into *true* values and then introduced in ABAQUS. Furthermore, the elastic Young's modulus and the Poisson's ratio are assumed to be 200,000 MPa and 0.3 in the finite element modeling analysis in the current study, respectively.

4. Results and discussion

All four girders failed in shear in the thinner web panel (with $t_w = 4$ *mm*). The location of the shear buckles changes between one of the two ends of this web panel. Given that the shear force within the web panel and the geometric properties remain constant, the change in buckling location can be attributed to initial imperfections.

As described in section 3.3, the full field geometry of the thinner web panel was scanned by 3D-DIC before the tests. Then, the DIC measured mesh (actual data) is compared against the perfect geometry (nominal data) in the GOM Inspect software to map the initial imperfections. The 3-point alignment is used as an initial alignment to bring the actual data closer to the nominal data and make them comparable. The results of such a comparison for all the four girders are shown in Fig. 8. The buckling deformations of the four girders are shown in Fig. 9. For girders 1002 and 1004, the shear buckles occurred close to the end support. By looking back to Fig. 8, it is observed that the geometric imperfections in these two girders are larger near the support than elsewhere in the panel. On the other hand, in 1001 and 1003, the imperfections are more intense at the end near the loading point in the middle of the girders, and consequently the buckles appear there as shown in Fig. 9.

It is worth mentioning that the initial imperfections of the web panels in Fig. 8 are shown on the reverse side of the girders in Fig. 9. In other words, the right end of the web panel in Fig. 8 is next to the load point in the middle, and the left end is adjacent to the end support, according to the specified coordinate axes.

4.1. The shear strength in the conducted tests vs. EN 1993-1-5

Fig. 10 depicts the mid-span vertical deflection against the total applied load for all four girders. The maximum applied load varies from 3503 kN in 1002 to 3188 kN in 1004, with a 9% difference. Table 2 shows the maximum shear force, V_{ult}, which is half of the total applied load in each girder. While all the girders have the same web height of $h_w = 1400\,mm$, 1004 is cut 100 *mm* shorter and has a web height of 1300 *mm*. considering that the buckled web panel in all the girders has the same thickness of $t_w = 4\,mm$, and the yield strength of the employed material, EN 1.4162/LDX 2101, is $f_{yw} = 460\,MPa$, the plastic shear force, V_P, is calculated according to Eq. (15). The shear yield stress, τ_y, is equal to $f_{yw}/\sqrt{3}$.

$$V_P = \tau_y h_w t_w \tag{15}$$

The ratio between the maximum shear force and the plastic shear

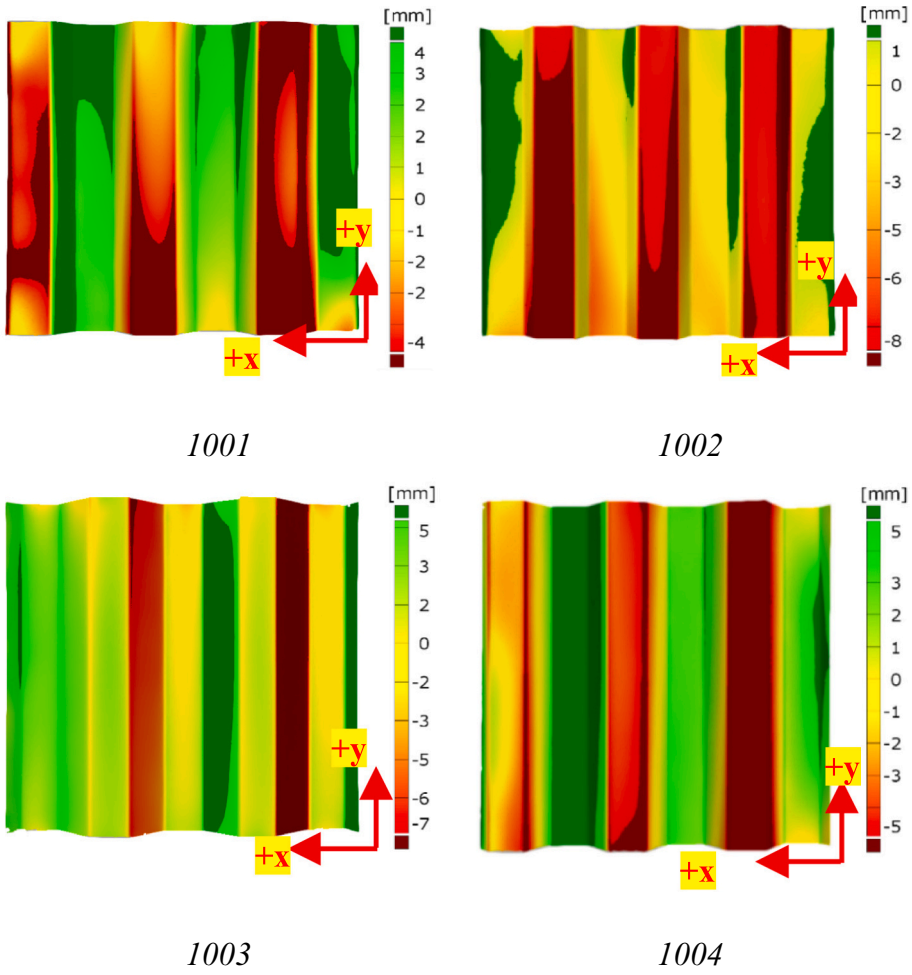

Fig. 8. Initial imperfection maps for thinner web plates of the tested girders; 1001–1004.

force, V_{ult}/V_P, which is equivalent to the ratio between the ultimate shear stress and the shear yield stress, τ_{ult}/τ_y, ranges from 1.08 to 1.18. This ratio is larger than 1 in all four girders, indicating that the ultimate shear stress exceeded the shear yield stress. So, not only do the girders not buckle prior to yielding, but their strength increases after yielding owing to the material's strain hardening effect. The maximum principal strain at ultimate load, $\varepsilon_{ult,max}$, calculated from strain measurements in triax-2 during the tests, is greater than the yield strain ($\varepsilon_y = 2300\ \mu m/m$) in all the girders, confirming that the shear strength of the girders surpasses the shear yield strength.

Table 2 shows the predicted EN 1993-1-5 local and global slenderness parameters, $\bar{\lambda}_{c,l}$ and $\bar{\lambda}_{c,g}$, respectively. The global slenderness parameters for all girders are less than 1. Therefore, the global buckling reduction factor according to the Eurocode model is $\chi_{c,g} = 1$ and there is no drop in shear strength in global buckling, indicating that the global buckling mode is not governing.

On the other hand, the local slenderness parameter for all the girders is approximately 0.7, which results in $\chi_{c,l} = 0.71$. This indicates that the local buckling is governing, and the ultimate shear strength is reduced with respect to the shear yield strength by applying $\chi_c = 0.71$ as the reduction factor. Part of this reduction is due to ignoring the effect of fixity at the web-flange junction in the design model aimed to provide lower bound results as discussed in section 2. However, the main reason for this strength reduction is the range of the local slenderness parameter. Fig. 2 shows that $\lambda = 0.7$ is in the medium range, in which EN 1993-1-5 does not allow to rely on the material yield strength due to, first, a lack of access to sufficient supporting experimental data and, second, a high sensitivity to initial imperfections. Although the ultimate shear stress in the stainless steel girders tested in this research exceeded the yield stress, an imperfection sensitivity analysis is required to evaluate the extent of the reduction in the Eurocode design shear strength compared to the yield stress. The finite element approach is used to explore the sensitivity of the shear behavior to initial imperfections, as explained in the section 4.3.

4.2. Nonlinear finite element vs. test results

The results of the first step of the finite element studies in which the girders are modeled with the critical web panels having the real measured geometry are discussed in this section. The fully nonlinear behavior beyond the ultimate load is analyzed via the Static-Riks method in ABAQUS. In Fig. 11, the FE mid-span vertical deflection vs. the applied load is plotted and compared to the experimental response for all four girders. It is observed that the initial stiffness, the ultimate load, and the deflection at failure obtained from the experiments and simulations agree very well. However, the deformations after reaching the maximum load cannot be monitored in the experiment due to the rapid mode of failure. The nonlinear FE-model can track the post-buckling path reasonably well, however.

The level of stress at the failure load, as illustrated in Fig. 12, represents the full yield in the web's material followed by strain-hardening. Such a conclusion is backed by the maximum principal strains, $\boldsymbol{\varepsilon}_{ult,max}$, calculated using the strain measurements during the tests, as shown in Table 2.

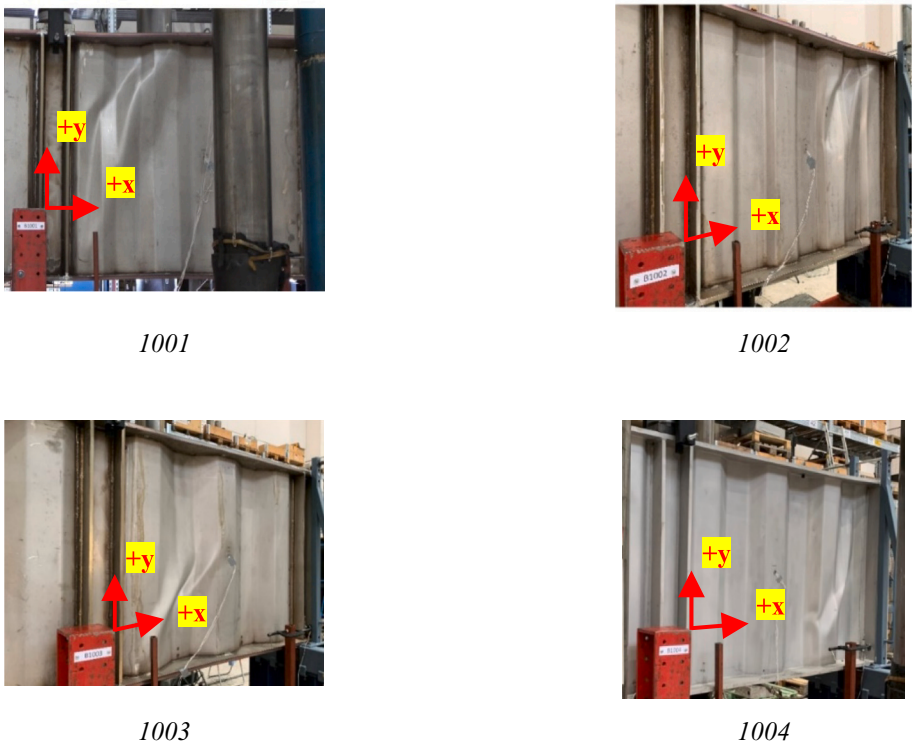

Fig. 9. Shear buckling deformation of the four tested girders; 1001–1004.

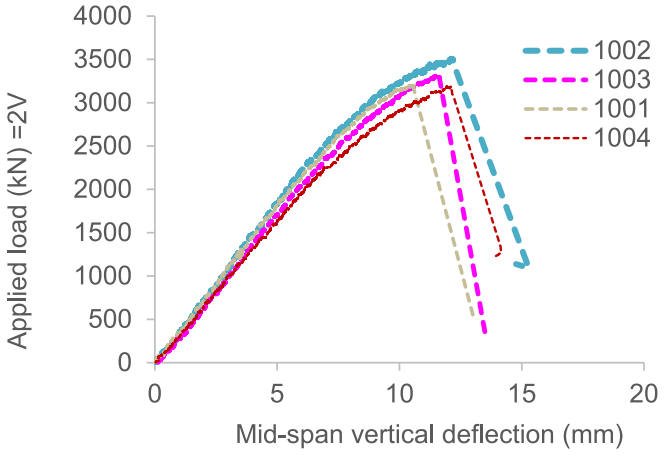

Fig. 10. Experimental load-displacement diagram for the girders, 1001–1004.

Table 2
Calculation of the shear strength based on the tests and according to EN 1993-1-5.

Girder's label	1001	1002	1003	1004
V_{ult} (kN)	1609	1751.5	1654.5	1594
h_w (mm)	1400	1400	1400	1300
V_P (kN)	1487	1487	1487	1381
V_{ult}/V_P or τ_{ult}/τ_y	1.08	1.18	1.11	1.15
$\varepsilon_{ult,max}$ $(\mu m/m)$	2327	3166	2971	3081
$\bar{\lambda}_{c,l}$	0.705	0.705	0.722	0.705
$\bar{\lambda}_{c,g}$	0.73	0.71	0.52	0.47

4.3. Analysis of the imperfection sensitivity

Even though the design of steel elements can be done using Geometrically and Materially Nonlinear Analysis (GNMA), the designer has, in general, no prior information about the mechanical and geometric imperfections of welded elements. As a solution, one typical method for considering the effect of initial imperfections is that an eigenvalue buckling analysis is performed on a finite element model with perfect geometry. The buckling deformation (one or a combination of buckling modes) with an equivalent maximum magnitude is included as an *equivalent* initial imperfection in a nonlinear analysis to account for the simultaneous effect of geometric imperfections and residual stresses. This method has been widely used for finite element studies on thin-walled structures and is proposed in many design standards, such as the Eurocodes.

A specificity of the shear buckling problem in corrugated plates is, as previously discussed in section 2, the different buckling modes that can be dominant. It is worth reminding that local buckling is characterized by distinct shear buckles within the individual corrugation folds. On the other hand, global buckling is characterized by shear buckles extending diagonally over the entire height of multiple adjacent folds. Finally, the distinctive feature of the so-called interactive buckling mode is the extension of local buckling half-waves onto adjacent folds.

In the second step of the current finite element studies, all four girders are modeled with perfect geometry and their eigen buckling modes are extracted. Based on the above characterization, the extracted buckling modes are then categorized as local or interactive/global. To start with, the first 10 buckling mode shapes of 1001 are extracted, scaled, and used as the initial shape in the nonlinear analysis steps. For the maximum amplitude of the imperfections, based on the collective recommendations from the literature review as stated in section 2, the three amplitudes of $h_w/200$, t_w and $a_{max}/200$ are considered in separate analyses. This gives in total 30 nonlinear analyses for this girder.

The FE shear strength of girder 1001 having different initial imperfections based on the different mode shapes and with different amplitudes is depicted in Fig. 13. It is observed that when the maximum amplitude of the imperfections is limited to $a_{max}/200$, i.e., 0.85 mm, the shear strength is, as expected, not very sensitive to the mode shape of the imperfection, and the buckling reduction factor, χ, is larger than 1. However, when the amplitude rises to $t_w = 4mm$ and $h_w/200 = 7mm$,

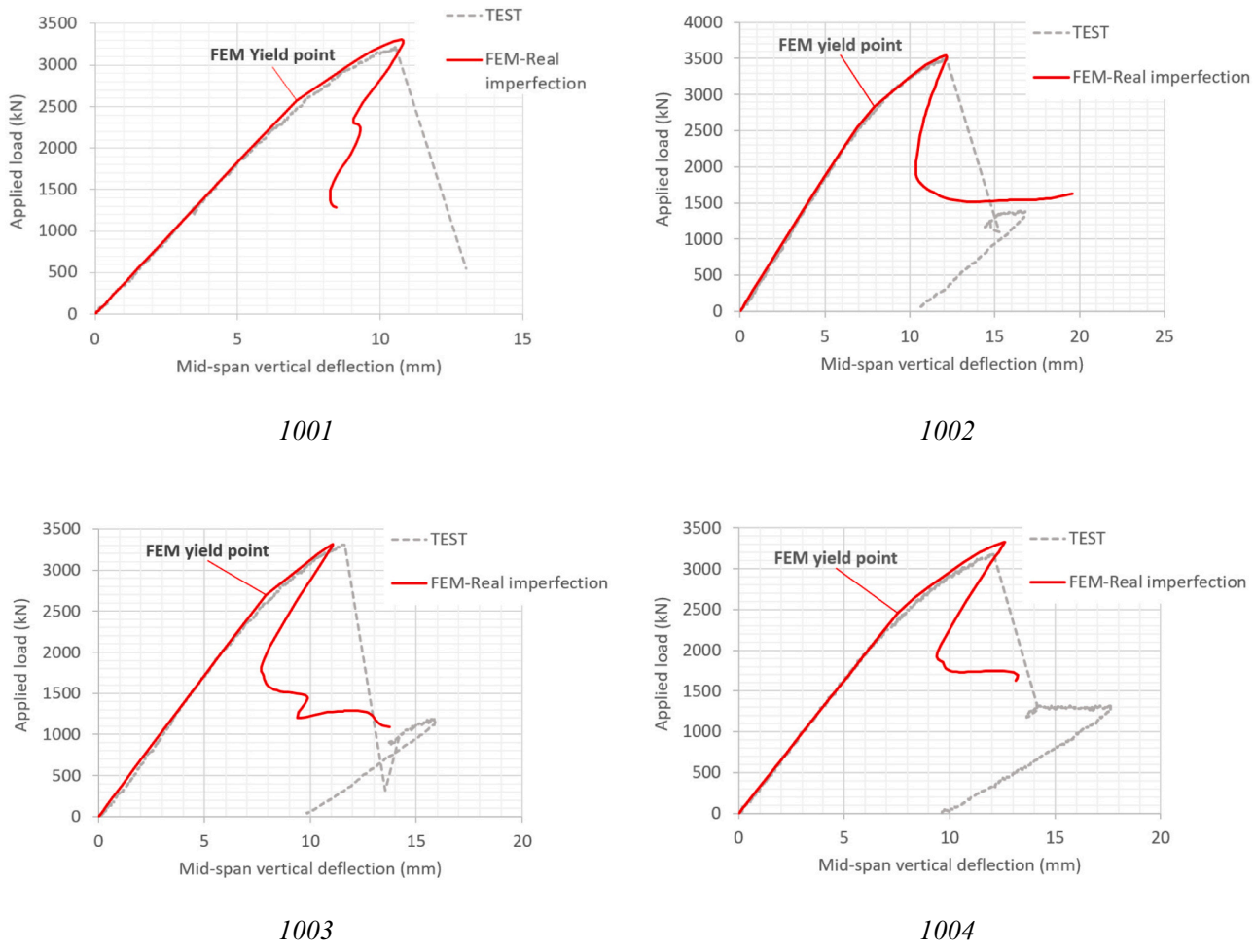

Fig. 11. Comparison between the load-displacement diagram obtained from the experimental and finite element studies.

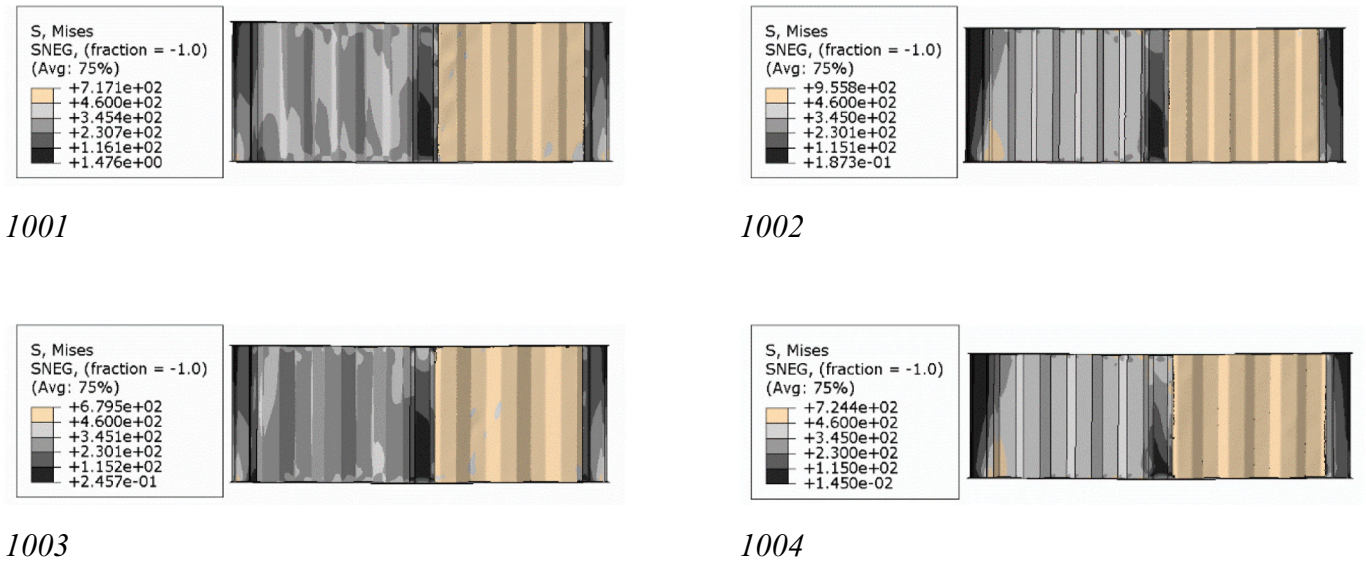

Fig. 12. State of stresses at the ultimate load; obtained from the finite element studies, the critical panels being on the left.

the shear strength is reduced considerably and becomes dependent on the mode shape chosen for imperfection. A comparison between the buckling reduction factors reveals that those mode shapes that are extended over only a limited area of the entire web (modes 3 and 4 in this case) result in the highest shear strengths. The buckling reduction factors for the case of mode 3 are all over 1 for the different studied imperfection amplitudes. On the other hand, the minimum buckling reduction factors are related to those mode shapes which are extended

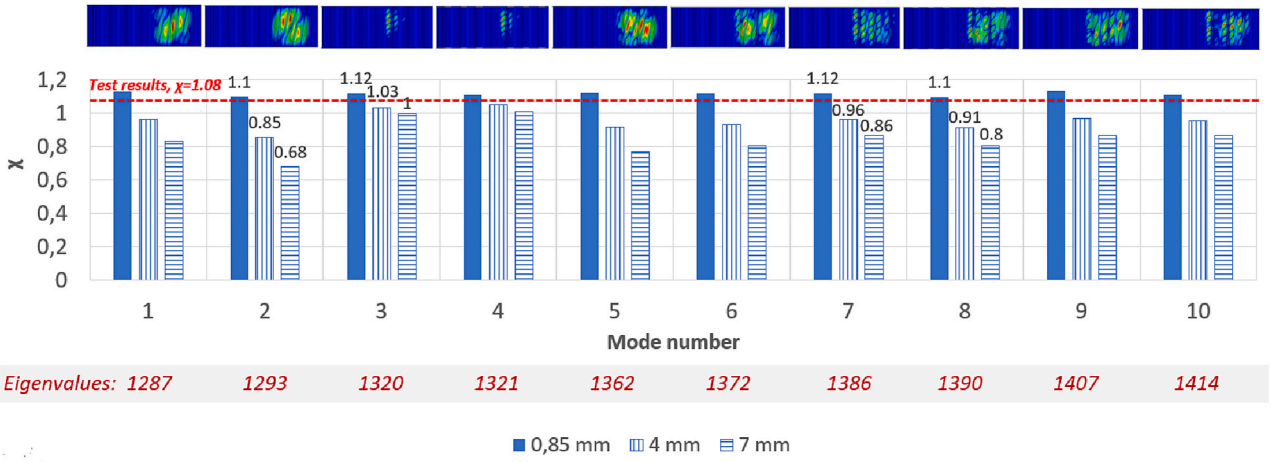

Fig. 13. FE shear strength the girder 1001 having initial imperfections in different mode shapes and with different amplitudes of 0.85 mm, 4 mm, and 7 mm.

over the entire web panel (modes 1, 2, and 5). It is observed that the second mode in this case gives the lowest buckling reduction factors, i.e., 0.85 and 0.68 for imperfection magnitudes of 4 mm and 7 mm, respectively. In the mode shapes where the extent of buckling deformations in the web panel is between the lower and upper limits (the last four modes), the buckling factors are also between the minimum and maximum values.

For the FE model of girder 1002, neglecting the similar mode shapes, the modes with different shapes in each of the two mentioned categories, local or interactive/global, have been extracted, see Fig. 14. It is observed that the first buckling mode is local and extends only over the folds adjacent to the support. Mode 13 is again a local mode, but this time extended over the entire web panel. The other two modes, 7 and 14, are categorized as interactive/global buckling modes.

The load-deflection curves for 1002 having different imperfections are plotted in Fig. 15. It is observed that the first local buckling mode (mode 1 in Fig. 14) with an amplitude of $a_{max}/200$ gives an ultimate load and deformation very close to the test result. This is confirmed by what has already been observed in Fig. 9, that buckling in this girder occurred locally at the end near the support.

Regardless of which mode shape and amplitude give the results which fall closest to the test result, what is essential from the design point of view is the minimum buckling strength, i.e., the case which results in the lowest ultimate load that can happen in a real girder. Like what was observed in the case of 1001, Fig. 15 shows that in girder 1002, the ultimate load is not very sensitive to the shape of the imperfection when small amplitudes of initial imperfections are used (i.e., 0.85 mm). But when the amplitude of the imperfection is increased to 4 mm or 7 mm, then it is clearly seen that the first buckling mode does not result in the minimum strength. Higher modes (modes 7, 13, and 14) give lower ultimate loads with the same amplitude of imperfection assigned to these modes. This can be an important observation since many previous studies have recommended using the first buckling mode with an equivalent amplitude of $h_w/200$ for the purpose of design. The highlight is that in a search among the considered buckling modes, it was found that those buckling modes which are extended over the entire web panel result in a lower strength, and that the larger the area over which the considered buckling mode extends, the lower the ultimate load. In the case of girder 1002, mode 7 results in the lowest shear strength with around 6% reduction with respect to the shear yield strength for an amplitude of 4 mm and 20% reduction for an amplitude of 7 mm.

The buckling mode shapes of the other two girders, i.e., 1003, and

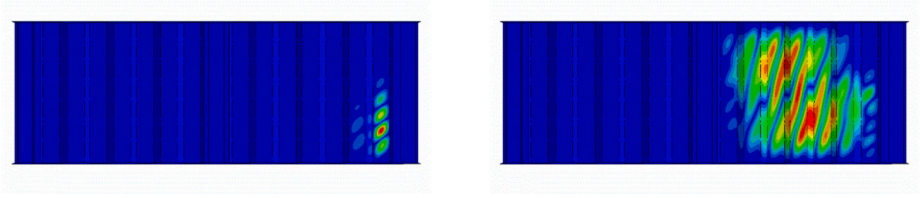

Mode 1-Local

Eigenvalue: 1277

Mode 7-Interactive/global

Eigenvalue: 1398

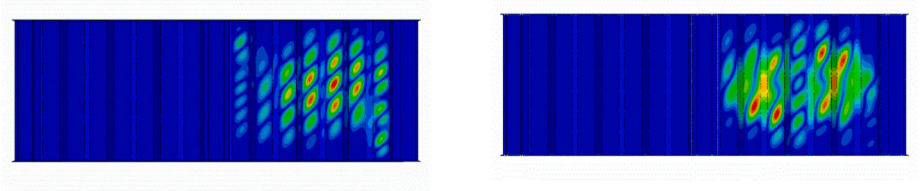

Mode 13- Local

Eigenvalue: 1456

Mode 14-Interactive/global

Eigenvalue: 1468

Fig. 14. Eigen buckling modes of 1002.

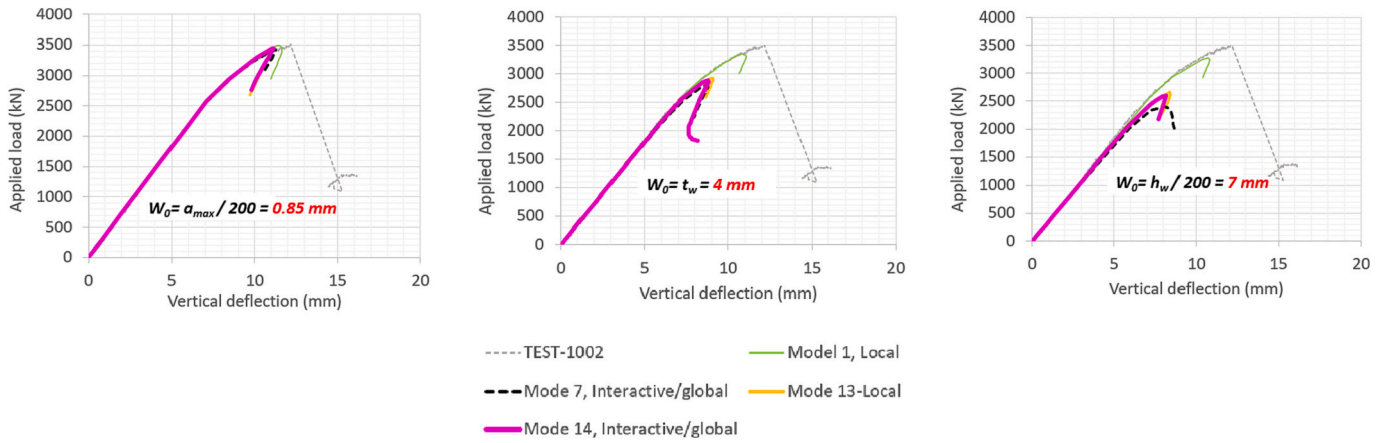

Fig. 15. FE load-deflection curve for 1002 with different initial imperfections vs. the test.

1004, are categorized as well and the non-linear behavior including different imperfections is studied in the same way as for 1001 and 1002. However, the load-deflection curves are not shown here for the sake of brevity. In Fig. 16 and Fig. 17, the ratio between the FE shear strength for all the four girders having different initial imperfections is depicted and compared to the EN 1993-1-5 design strength. It is again observed that regardless of the mode shape or the mode number, a mode that is locally extended over a limited area of the web panel and has a maximum amplitude of $a_{max}/200$ gives the highest ultimate shear strength and is closest to the test results. This is modes 35 and 1, in girders 1003 and 1004 respectively.

In Fig. 16 it is observed that including a small initial imperfection of $a_{max}/200$ results in a shear strength which is higher than the yield strength ($\chi = 1$) independent of the mode shape. However, when the amplitude rises to t_w and $h_w/200$, 4 mm and 7 mm, respectively, then the shear strength obtained with most mode shapes is lower than the shear yield strength with the difference ranging between 13 and 30%. However, even with an amplitude of $h_w/200$, which according to previous

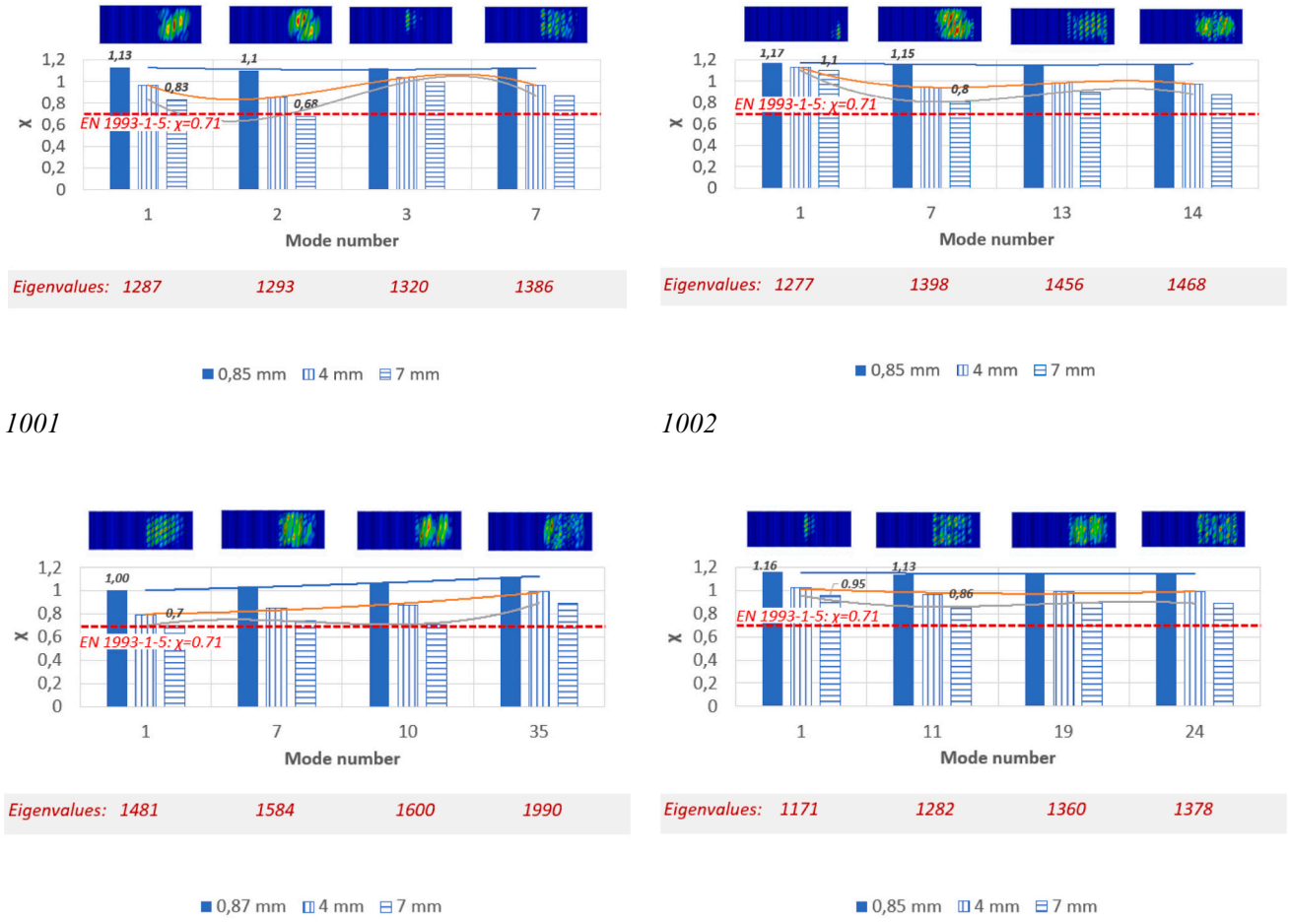

Fig. 16. Ratio between the FE shear capacity of the girders with different initial imperfections and the shear yield strength.

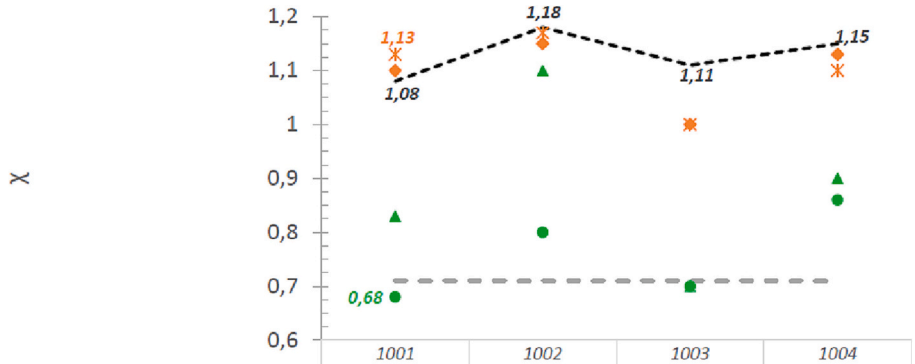

	1001	1002	1003	1004
mode 1, amax/200	1,13	1,17	1	1,1
The critical mode, amax/200	1,1	1,15	1	1,13
Test results	1,08	1,18	1,11	1,15
The Eurocode buckling reduction factor	0,71	0,71	0,71	0,71
mode 1, hw/200	0,83	1,1	0,7	0,9
The critical mode, hw/200	0,68	0,8	0,7	0,86

Fig. 17. Shear buckling factors obtained from imperfection sensitivity studies in comparison to the conducted tests and the Eurocode design model.

studies, e.g., [8], may be a large and unrealistic amplitude in corrugated web girders, the shear strength is higher than the EN 1993-1-5 design strength ($\chi = 0.71$) in most of the studied cases.

Based on the results presented in Fig. 16 and Fig. 17, the common recommendation in design to consider the first buckling mode and with a maximum amplitude of $h_w/200$ is evaluated. This recommendation did not lead to lower buckling factors compared to the Eurocode design model. However, if the comparison is made based on the test results, such a recommendation can be very conservative. All tested girders showed, as reported in the experimental studies section, a greater strength than the shear yield strength. On the other hand, it is observed that considering an initial imperfection based on the first buckling mode with a maximum amplitude of $a_{max}/200$ leads to a buckling reduction factor, χ in Fig. 16 and Fig. 17, which is higher than 1, which agrees better with the test results, V_{ult}/V_P in Table 2.

By comparing the eigenvalues in relation to the buckling reduction factors as shown in Fig. 16, it is observed that the buckling reduction factors are not necessarily proportional to the eigenvalues. For example, in the case of 1001, a comparison between modes 2, 3, and 7 reveals that although the third eigenvalue is slightly higher than the second eigenvalue, the buckling reduction factor for an imperfection magnitude of 7 mm, for example, increases from approximately 0.7 in mode 2 to 1 in mode 3. On the other hand, for mode 7, which has a slightly higher eigenvalue than the third mode, the buckling factors are less. Upon this observation, the previous conclusion about the dependence of the buckling factor and the ultimate shear strength on the extent of the buckling deformations and not the mode number or the eigenvalue in the studied girders is confirmed.

The interactive buckling mode shape is not taken into consideration in EN 1993-1-5 owing to what is believed to be a weak interaction between local and global modes. The present investigation confirms this idea by comparing mode shapes 13 and 14 in girder 1002 in Fig. 16. Although the mode shape changes from local in mode 13 to interactive in mode 14, there is no noticeable shift in the buckling reduction factors. A similar conclusion may be reached by comparing girder 1004 results for modes 19 and 24. This seems to be the case since yielding occurs prior to buckling, and the influence of buckling modes is proportional to the extent of buckling deformation in the web panel, which is not significantly different between the compared cases.

5. Conclusions

The current study's shear tests on four corrugated web girders made of EN 1.4162/LDX 2101 stainless steel show an ultimate shear strength greater than the shear yield strength for a local slenderness ratio of around 0.7. This slenderness ratio is much beyond the limit of $\lambda = 0.25$ in the Eurocode. It is worth noting that the Eurocode's limit of $\lambda = 0.25$ on the slenderness is due to the lack of enough experimental data showing that girders with higher slenderness ratios can reach yielding and the high imperfection sensitivity. In the case of the stainless steel girders in the current research, the high imperfection sensitivity of the ultimate shear resistance to the initial imperfections is also observed. However, as discussed in Section 4.1 and Fig. 17, all the girders reached stress levels higher than the shear yield stress. This is clearly attributed to the high capacity of stainless steel for strain hardening and the fact that the increase in the ultimate shear capacity due to the strain hardening compensates part of the reduction in the capacity due to the presence of initial imperfections, and the shear resistance of stainless steel girders can attain yielding within a wider range of slenderness ratios. Therefore, the Eurocode's limit can be quite conservative for stainless steel corrugated web girders within the medium range of slenderness ratios.

On the other hand, the results of the imperfection sensitivity studies with the aid of FEM reveal that when the amplitude of the initial imperfection is limited to the minimum dimension of the critical corrugation sub panel, a_{max}, divided by 200, the sensitivity of the ultimate shear strength to the mode shape is negligible, the results are very close to the test results, and the shear yield strength is achieved. By increasing the amplitude of the imperfection to the thickness of the plate, t_w, or $h_w/200$, the sensitivity of the ultimate load to the mode shape is more pronounced in a way that mode shapes that are more extended over the web panel, regardless of the mode number, cause more degradation of the ultimate shear strength. This information could influence the FEM-based design of corrugated web girders.

On the other hand, the recommendation of assuming an equivalent initial imperfection with an amplitude of $h_w/200$ is found to be conservative for the tested girders in this study. For the other studied amplitude, i.e., t_w, it is found that the variation of the buckling strength with respect to the yield strength is in the range of −20% to +12% for the tested girders, which seems more reasonable.

In the current investigations, it is clearly shown that the variation of the ultimate shear strength is strongly dependent on the amplitude of the

imperfection in addition to what was previously described as the extent of the buckling deformations over the web panel. For the tested girders in the current study, it is observed that assuming an initial imperfection based on the first eigen buckling mode to a maximum amplitude of $a_{max}/200$ leads to an ultimate shear strength larger than the shear yield strength and close to the test results. It is believed that the next important step to advance the current research is first to conduct studies to determine an accurate model to take into account the initial imperfections in corrugated plates and then to determine the production tolerances for the maximum allowed amplitude of the imperfections, which was not within the scope of the current study. Then, based on such a model and the conclusions in the current studies, extensive parametric studies should be carried out with the aim of verifying and updating the current design models in Eurocode for use in stainless steel.

CRediT authorship contribution statement

Mozhdeh Amani: Methodology, Software, Validation, Formal analysis, Investigation, Data curation, Writing – original draft, Visualization. **Mohammad Al-Emrani:** Conceptualization, Methodology, Investigation, Resources, Writing – review & editing, Supervision, Project administration, Funding acquisition. **Mathias Flansbjer:** Data curation, Writing – original draft.

Declaration of Competing Interest

The authors declare that they have no known competing financial interests or personal relationships that could have appeared to influence the work reported in this paper.

Data availability

Data will be made available on request.

Acknowledgement

The research work reported in this paper was conducted within the research project “Sunlight,” which was funded by the Swedish Innovation Agency, VINNOVA, and LIGHTer during the period 2019–2022. The Swedish Transport Administration (Trafikverket), the Swedish Institute of Steel Construction (SBI), SWERIM, COWI, WSP, ESAB, Stål och Rörmontage, and Outokumpu all made valuable contributions to the project. All the contributions are much appreciated.

References

[1] Design Manual for Structural Stainless Steel, 4th edition, Berkshire, Silwood Park, Ascot, 2017. SL5 7QN UK: SCI.
[2] Robert G. Driver, Hassan H. Abbas, Richard Sause, Shear behavior of corrugated web bridge girders, J. Struct. Eng. 132 (2) (2006) 195–203.
[3] Mohamed Elgaaly, Robert W. Hamilton, Anand Seshadri, Shear strength of beams with corrugated webs, J. Struct. Eng. 122 (4) (1996) 390–398.
[4] M.F. Hassanein, A.A. Elkawas, A.M. El Hadidy, Mohamed Elchalakani, Shear analysis and design of high-strength steel corrugated web girders, Eng. Struct. 146 (2017) 18–33, https://doi.org/10.1016/j.engstruct.2017.05.035.
[5] M.F. Hassanein, O.F. Kharoob, Behavior of bridge girders with corrugated webs: (I) real boundary condition at the juncture of the web and flanges, Eng. Struct. 57 (2013) 554–564, https://doi.org/10.1016/j.engstruct.2013.03.004.
[6] T. Höglund, Shear buckling resistance of steel and aluminium plate girders, Thin-Walled Struct. 29 (1997) 13–30.
[7] B. Johansson, R. Maquoi, G. Sedlacek, C. Müller, D. Beg, Commentry and Worked Example to EN 1993-1-5 “Plated Structural Elements”, Scientific and technical reports, European Communities, Luxembourg, 2007.
[8] D. Kollár, B. Kövesdi, Welding simulation of corrugated web girders - part 2: effect of manufacturing on shear buckling resistance, Thin-Walled Struct. 141 (2019) 477–488, https://doi.org/10.1016/j.tws.2019.04.035.
[9] Moussa Leblouba, M. Talha Junaid, Samer Barakat, Salah Altoubat, Mohamed Maalej, Shear buckling and stress distribution in trapezoidal web corrugated steel beams, Thin-Walled Struct. 113 (2017) 13–26, https://doi.org/10.1016/j.tws.2017.01.002.
[10] Moussa Leblouba, Samer Barakat, Zaid Al-Saadon, Shear behavior of corrugated web panels and sensitivity analysis, J. Constr. Steel Res. 151 (2018) 94–107, https://doi.org/10.1016/j.jcsr.2018.09.010.
[11] Jiho Moon, Jongwon Yi, Byung H. Choi, Hak-Eun Lee, Shear strength and design of trapezoidally corrugated steel webs, J. Constr. Steel Res. 65 (2009) 1198–1205, https://doi.org/10.1016/j.jcsr.2008.07.018.
[12] Jian-Guo Nie, Li Zhu, Mu-Xuan Tao, Liang Tang, Shear strength of trapezoidal corrugated steel webs, J. Constr. Steel Res. 85 (2013) 105–115, https://doi.org/10.1016/j.jcsr.2013.02.012.
[13] Mattias Renström, Oskar Rydh, Analysis of High Strength Stainless Steel in Road Bridges, Division of Structural Engineering, Chalmers University of Technology, 2014.
[14] Barbara Rossi, Discussion on the use of stainless steel in constructions in view of sustainability, Thin-Walled Struct. 83 (2014) 182–189, https://doi.org/10.1016/j.tws.2014.01.021.
[15] Richard Sause, Thomas N. Braxtan, Shear strength of trapezoidal corrugated steel webs, J. Constr. Steel Res. 67 (2011) 223–236, https://doi.org/10.1016/j.jcsr.2010.08.004.
[16] Richard Sause, Hassam H. Abbas, Wagdy G. Wassef, Robert G. Driver, Mohamed Elgaaly, Corrugated Web Girder Shape and Strength Criteria, ATLSS Reports, ATLSS report number 03-18, http://preserve.lehigh.edu/engr-civil-environmental-atlss-reports/245, 2003.
[17] Erik Schedin, Andy Backhouse, Stainless Steel Composite Bridge Study– A Summary of ARUP Reports, 2019. Outokumpu.
[18] Mohamed Soliman, Dan M. Frangopol, Life-cycle cost evaluation of conventional and corrosion-resistant steel for bridges, J. Bridge Eng. ASCE 20 (1) (2015), https://doi.org/10.1061/(ASCE)BE.1943-5592.0000647.
[19] Jeanette Säll, Anna Tiderman, Maintenance-Free Material in Bridge Superstructures, KTH, School of Architecture and Civil Engineering, 2013.
[20] EN 1993-1-5, In Eurocode 3: Design of Steel Structures-Part 1–5: Plated Structural Elements, CEN, 2005.
[21] EN 1993-1-4, In Eurocode 3: Design of Steel Structures-Part 1–4: General Rules-Supplementary for Stainless Steels, CEN, 2006.